

# Moving Towards Centers: Re-ranking with Attention and Memory for Re-identification

Yunhao Zhou, Yi Wang, *Member, IEEE*, and Lap-Pui Chau, *Fellow, IEEE*

**Abstract**—Re-ranking utilizes contextual information to optimize the initial ranking list of person or vehicle re-identification (re-ID), which boosts the retrieval performance at post-processing steps. This paper proposes a re-ranking network to predict the correlations between the probe and top-ranked neighbor samples. Specifically, all the feature embeddings of query and gallery images are expanded and enhanced by a linear combination of their neighbors, with the correlation prediction serves as discriminative combination weights. The combination process is equivalent to moving independent embeddings toward the identity centers, improving cluster compactness. For correlation prediction, we first aggregate the contextual information for probe’s  $k$ -nearest neighbors via the Transformer encoder. Then, we distill and refine the probe-related features into the Contextual Memory cell via attention mechanism. Like humans that retrieve images by not only considering probe images but also memorizing the retrieved ones, the Contextual Memory produces multi-view descriptions for each instance. Finally, the neighbors are reconstructed with features fetched from the Contextual Memory, and a binary classifier predicts their correlations with the probe. Experiments on six widely-used person and vehicle re-ID benchmarks demonstrate the effectiveness of the proposed method. Especially, our method surpasses the state-of-the-art re-ranking approaches on large-scale datasets by a significant margin, i.e., with an average 3.08% CMC@1 and 7.46% mAP improvements on **VERI-Wild**, **MSMT17**, and **VehicleID** datasets.

**Index Terms**—Re-Identification, transformer, attention, re-ranking, contextual memory.

## I. INTRODUCTION

Recently, re-identification (re-ID) tasks have drawn increasing interest in the computer vision society. Given an image from the query set, re-ID aims at finding all images containing the same instance as the query across a large gallery image set. In general, query and gallery images are captured by different cameras in multiple scenes. Thus, re-ID is often considered a sub-problem of image retrieval at the instance-specific level. Re-ID has a wide variety of applications according to the target instances. For example, person re-ID helps the criminal investigation [1] by looking for suspected persons with city surveillance cameras. Vehicle re-ID can analyze traffic [2], which is a crucial part of intelligent transportation systems in smart cities. The problem setting that retrieving instances from multiple non-overlapping cameras brings many challenges, such as varying viewpoints, illumination changes, occlusions, low-image resolutions, and cluttered backgrounds. Therefore, the key to re-ID is building robust and discriminative feature

Yunhao Zhou, Yi Wang, and Lap-Pui Chau are with School of Electrical and Electronics Engineering, Nanyang Technological University, Singapore, 639798 (e-mail: zh0022ao@e.ntu.edu.sg, wang1241@e.ntu.edu.sg, elpchau@ntu.edu.sg). Corresponding author: Lap-Pui Chau.

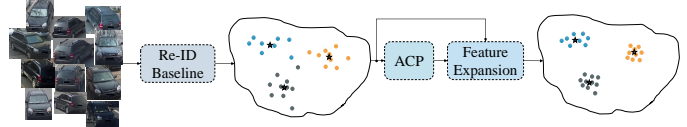


Fig. 1. General pipeline of re-ID and our Attention-based Correlation Predictor (ACP). Embeddings and identities are shown with dots and colors. Our re-ranking method aggregates each embedding and the corresponding  $k$ -nearest neighbors with predicted correlations, which moves independent embeddings towards the identity centers marked with stars.

embeddings to minimize intra-identity distance and maximize inter-identity discrepancy. As shown in Fig. 1, a re-ID baseline maps images to an embedding space. Early research mainly focused on designing hand-crafted image descriptors [3], [4]. As more and more training data becomes available, the ability of Convolution Neural Networks (CNN) to learn robust feature representations from data pushes the re-ID performance to a new level [5]–[7].

Basic re-ID models retrieve instances with pairwise distance measure, which only considers individual characters between two separate images at a time. Performance degrades quickly in challenging scenarios where images containing the same instance cannot be embedded into a small cluster and are not close enough to each other. To overcome the drawbacks of the pairwise matching rule, re-ranking leverages the contextual information in local neighbors to optimize the initial ranking list of re-ID, which conducts retrieval by integrating information from multiple images. For example, [8]–[10] aggregates the contextual information via directly averaging local neighboring embeddings. It is equivalent to substitute the pairwise distance with an overall distance between different groups of embeddings. Some methods resort to more complex rules like common nearest neighbors [11] or  $k$ -reciprocal neighbors [12]. Re-ranking has been integrated into many re-ID methods [5], [13], [14] because of the performance boost it brings, especially on mean Average Precision (mAP). However, most existing re-ranking approaches rely on hand-designed algorithms to leverage contextual information. They lack the ability to handle complex neighborhood relationships, which yields unsatisfying results on large-scale datasets. Moreover, some re-ranking methods are time-consuming. For example, the  $k$ -reciprocal re-ranking [12] calculates  $k$ -reciprocal neighbors of each probe image to form a new Jaccard distance. Experiments on the largest test set of **VERI-Wild** show that it takes more than 900s and 150GB RAM to finish re-ranking.

Given an initial ranking list from a re-ID baseline, humans achieve re-ranking by gradually verifying the retrieved images

and memorizing the appearance information of the verified confident samples. Our brain can summarize the scattered contextual information to form an overall description of a person or vehicle. Based on this observation, we propose a Contextual Memory cell to fulfill the information aggregation purpose powered by attention mechanism. We later reconstruct top-ranked samples by comparing their features with the refined Contextual Memory. Because falsely retrieved samples share less common features with the memory, their reconstruction results will be different from those true matches, which can be used for correlation prediction, i.e., whether a retrieved sample is a true match for the probe image. With the predicted correlations, we can shrink the independent feature embeddings to the identity centers through a weighted combination of their local neighbors in the original embedding space. An overview of our re-ranking model is visualized in Fig. 1 where the improved cluster compactness can reduce false matches. Specifically, we re-formulate the re-ranking as a binary classification problem of the top- $k$  retrieved samples and propose an Attention-based Correlation Predictor (ACP) to predict the correlations. The correlation prediction consists of three key steps. In the first step, each probe's  $k$ -nearest neighbors are fed into a Transformer encoder to aggregate the contextual information. Second, a Contextual Memory initialized by attention mechanism distills the probe-related contextual features. We further refine the memory with a small group of highly confident samples for the purpose of eliminating feature pollutions brought by interfering false matches. Third, we reconstruct neighbor embeddings with features fetched from the memory cell through Multi-Head Attention. A binary classifier with sigmoid activation predicts the correlation between each reconstructed neighbor embedding and the probe.

The proposed method is evaluated on six widely used benchmarks including VERI-Wild [15], MSMT17 [16], VehicleID [17], VeVi [18], Market1501 [19] and DukeMTMC [20]. Experimental results show that our method surpasses state-of-the-art re-ranking methods by a large margin on large-scale benchmarks VERI-Wild, MSMT17, and VehicleID. For smaller benchmarks with limited training images, we ranked high amongst the competing methods. Ablation study verifies the effectiveness of our Contextual Memory and refinement process. In summary, the contribution of this paper is three-fold:

- We propose to use the Contextual Memory cell to mimic the remembering process that humans adopt for re-ID and re-ranking. Embeddings obtained from single-view images are expanded with attention mechanism, which learns to focus on the most discriminative regions.
- We reformulate re-ranking as a binary classification problem. The independent embeddings are moved to the identity centers by combining local neighbors with correlation prediction produced by the classifier.
- Extensive experiments on six re-ID datasets demonstrate the superiority of the proposed method. Detailed model studies reflect how each module and parameter affect the performance.

## II. RELATED WORK

### A. Deep feature representation of re-ID

Recently, CNN-based feature representation learning has achieved great success on re-ID tasks. In the early years, many re-ID methods [21], [22] with deep learning techniques directly learn a global feature embedding from the whole image. However, a single global feature often fails to distinguish two similar-looking instances like vehicles in the same model or persons dressed in the same color and style. To solve this problem, some methods extract supplementary features like strong discriminative regions [6], viewpoints [7], [23] or attribute characteristics [24] to provide auxiliary cues for the global feature. For example, the Part-based Convolutional Baseline (PCB) [13] uniformly partitions the learned feature map into multiple horizontal stripes. Strip features provide part-level information from different body regions. Zhou *et al.* [7] combined CNN with Long Short-Term Memory (LSTM) to learn the transformations across different viewpoints of vehicles. Multi-view vehicle representation can be inferred from a single view image input. Instead of focusing on model architectures, another line of work adopts metric learning methods to improve the feature discriminability. Hermans *et al.* [25] proposed a variant of triplet loss with batch hard sampling strategy to pull positive samples together and push negative samples away. It has become one of the most common choices [5], [6] to train deep re-ID networks supervised by the combination of triplet loss and cross-entropy identity loss.

### B. Re-ranking for re-ID and Image Retrieval

Re-ranking plays a crucial role in improving retrieval performance at post-processing steps. Given an initial ranking list, re-ranking refines the result utilizing contextual information in top-ranked samples. Although feature representation learning ushers in the blossom of deep neural networks, most existing re-ranking methods still stagnate in hand-designed rules when analyzing the relations between neighboring embeddings. Chum *et al.* [8] proposed Average Query Expansion (AQE) for image retrieval tasks, which replaces query feature embeddings with the mean of top- $k$  retrieved gallery samples. Instead of taking the mean average, Radenović *et al.* [9] resort weighted average named alpha Query Expansion ( $\alpha$ QE). The weights are calculated by taking the power of similarity between the query and top- $k$  retrieved samples with an exponent as a hyper-parameter  $\alpha$ . Because of its simplicity and robustness,  $\alpha$ QE has been adopted as a common approach of boosting retrieval performance by a number of image retrieval and re-ID works. To improve the discriminability, Arandjelović *et al.* [10] proposed Discriminate Query Expansion (DQE) which trains a linear Support Vector Machine (SVM) with top-ranked and bottom-ranked samples as positive and negative samples, respectively. The distances between samples and the decision boundary work as pseudo labels to aggregate the  $k$ -nearest neighbors. Direct utilization of top-ranked samples faces the challenge of false-match pollution. Qin *et al.* [26] first proposed  $k$ -reciprocal nearest neighbors to eliminate outliers. Two images are called  $k$ -reciprocal nearest neighbors if they both ranked top- $k$  when the other image serves as a probe. Bai

and Bai [27] proposed Sparse Contextual Activation (SCA) which encodes the local distribution of an image in contextual space. Zhong *et al.* [12] calculate the expanded  $k$ -reciprocal nearest neighbor sets whose Jaccard distance is aggregated with the original distance via convex combination. Expanded Cross Neighbor (ECN) is introduced by [23] which sums the distances of images in expanded neighbors. Yu *et al.* [28] divide the extracted features into multiple sub-features, then the contextual information is iteratively encoded and fused into new feature vectors. Ye *et al.* [1] proposed to consider not only the similarity of top- $k$  samples but also the dissimilarity of bottom- $k$  samples from different baseline methods. Recently, Wang *et al.* [29] proposed reciprocal optimization that takes multiple queries into account.

The continuous progress of re-ranking methods pushes the performance forward by designing more and more sophisticated algorithms when exploiting the contextual information hiding in  $k$ -nearest neighbors. Hand-designed rules generalize well on small benchmarks but show difficulties in fitting large amounts of data. Zhang *et al.* [30] proposed to use graph convolutional network for link probability prediction and replace the original Euclidean distance with the predicted probability. Instead, we consider our correlation prediction as combination weights to shrink independent embeddings toward their identity centers. Therefore, we are not suffered from predicting the entire pairwise correlations between queries and galleries. Besides, our method only requires finding the first-order neighbors for each embedding. The whole architecture can be easily implemented under existing deep learning frameworks with GPU acceleration available painlessly.

### C. Attention and Transformer

Transformers were introduced by [31] and have achieved huge success on a wide range of natural language processing tasks. The core idea of Transformer is to update the sequence with information aggregated from the entire input sequence via attention mechanism which captures complex relationships between different input tokens. Recently, Transformer starts to shine in computer vision society. Wang *et al.* [32] proposed Non-local Neural Networks that use self-attention to aggregate image feature representations from non-local regions. Parmar *et al.* [33] leverage the self-attention of Transformer for auto-regressive image generation. Carion *et al.* [34] proposed Detection Transformer (DETR) with self-attention layers built on top of convolutional backbones. Dosovitskiy *et al.* [35] proved Vision Transformer (ViT) can achieve state-of-the-art performance on image recognition tasks, which relies on self-attention with flattened image patches as inputs discarding the convolutional architecture entirely. For re-ID, TransReID proposed by [36] shows that the self-attention between image patches can produce more robust features than CNN because information loss on details is avoided by removing convolution and downsampling operators. In this work, the self-attention of Transformer is used to explore the contextual information in local neighborhoods.

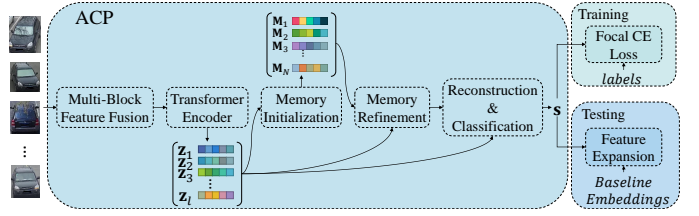


Fig. 2. Architecture of our Attention-based Correlation Predictor.

## III. OUR APPROCH

In this section, we first formulate the re-ID baseline and re-ranking with feature expansion in Section III-A. Next, the detailed model architecture is described in Section III-B. We visualize the pipeline of our re-ranking approach, named Attention-based Correlation Predictor (ACP), in Fig. 2.

### A. Overview of re-ID and re-ranking

Given an image from the query set, re-ID aims at retrieving images containing the same instance in the gallery set. Re-ID first maps images to  $D$ -dimensional vectors through a feature extractor  $\phi$ . We define the feature representation of images as  $\mathbf{f} = \phi(\mathcal{I})$ . The output feature vectors form two matrices:  $\mathcal{Q} \in \mathcal{R}^{M \times D}$  and  $\mathcal{G} \in \mathcal{R}^{N \times D}$  where  $M$  and  $N$  refer to the number of images in query and gallery sets, respectively. Then, pairwise distances between the feature representations in  $\mathcal{Q}$  and  $\mathcal{G}$  are calculated. The retrieval process of re-ID is achieved by sorting the distances in ascending order. It is expected that images holding the same instances will group together in the embedding space, so the correct matches in the gallery set will be ranked closer to the query.

Our re-ranking network exploits the contextual information in top-ranked samples to optimize the initial ranking list produced by the re-ID baseline. Given an image, we expand its embedding  $\mathbf{p}$  with the linear combination of its  $k_1$ -nearest neighbors (including itself). The weights are predicted by our ACP as shown in Fig. 2. The expansion moves independent embeddings toward their identity centers, which boosts the performance because of the improved cluster compactness. Denote the embeddings of  $k_1$ -nearest neighbors of  $\mathbf{p}$  as  $\mathbf{N}_f = \{\mathbf{f}_i\}_{i=1}^{k_1}$ , and the corresponding original images as  $\mathbf{N}_I = \{\mathbf{I}_i\}_{i=1}^{k_1}$ . The feature expansion of  $\mathbf{p}$  is,

$$\mathbf{p}^* = \sum_{j=1}^{k_1} \mathbf{N}_f^j \odot \mathbf{s}_j \quad (1)$$

where  $\mathbf{s} = \text{ACP}(\mathbf{N}_I)$ ,  $\mathbf{s} \in \mathcal{R}^{k_1}$  and  $\odot$  is element-wise product. Note that we perform feature expansion for both the query and gallery sets. Finally, the pairwise distances between updated embeddings in two sets are re-calculated and sorted to accomplish the instance re-ID goal.

### B. Model Architecture for Re-ranking

Given an image, we sort its  $k_1$ -nearest neighbors into a sequence. The attention is a powerful tool in aggregating contextual information over the sequence, while the Contextual Memory can distill the probe-related features for correlation

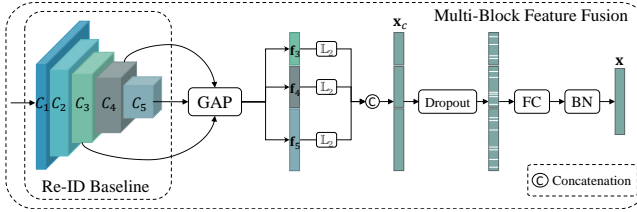


Fig. 3. Multi-Block Feature Fusion. The colored cuboids represent features from different blocks of the backbone ResNet-50 [37]. GAP is a global average pooling layer. FC and BN are fully connected layer and Batch Normalization layer, respectively.

prediction, which are integrated into the ACP. In this section, we first describe a multi-block feature fusion module. Then, we elaborate on how Contextual Memory is initialized and how the correlations are predicted via attention and the memory modules.

1) *Multi-Block Feature Fusion*: We visualize the feature fusion module in Fig. 3. The feature extractor of the re-ID baseline is ResNet-50 [37] which consists of 5 blocks, i.e.,  $C_1, C_2, C_3, C_4$ , and  $C_5$ . Feature maps from successive two blocks have a stride difference of 2. The re-ID baseline model obtains image embeddings by feeding  $C_5$  through a global average pooling (GAP) layer to reduce the spatial dimension. The features from shallower layers are discarded. Instead of following this routine, we propose a multi-block feature fusion module to fuse the features from different blocks because they provide complementary information to each other.

Suppose the multi-block features for an image  $\mathcal{I}$  as  $\phi(\mathcal{I}) = \{f_1, f_2, \dots, f_5\}$ , where  $f_j$  is  $j$ -th feature vector generated by performing global average pooling on CNN feature maps. For ResNet-50, we fuse the last three pooled feature vectors, i.e.,  $\{f_3, f_4, f_5\}$ . The feature vectors are first normalized by  $L_2$  normalization and rescaled with a learnable scale parameter. The scaled  $L_2$  normalization layer is formulated as,

$$\hat{f}_j = \frac{f_j}{\|f_j\|_2} \odot \gamma \quad (2)$$

where  $\|\cdot\|_2$  is the  $L_2$  norm of a vector. The normalized feature vectors  $\{\hat{f}_3, \hat{f}_4, \hat{f}_5\}$  are concatenated into  $x_c \in \mathcal{R}^{d_c}$ . To prevent over-fitting and improve generalization ability, a Dropout layer with dropout rate as  $p_d$  is placed after the normalization. Feature fusion is done with a fully connected layer followed by Batch Normalization (BN).

$$x = \text{BN}(\text{Dropout}(x_c)W + b), \quad x \in \mathcal{R}^d \quad (3)$$

where  $x$  is the fused feature vector for image  $\mathcal{I}$ , and  $d$  is the embedding dimension of  $x$ .

2) *Context Aggregation via Transformer*: Although the multi-block feature fusion fuses information from different layers, the feature vector  $x$  only captures the appearance of an independent image. To aggregate contextual cues in multiple images, we feed the sequence (sorted  $k_1$  nearest neighbors) into a Transformer encoder composed of Multi-Head Attention (MHA) and feed-forward networks (FFN). The Transformer encoder is visualized in Fig. 4.

In MHA, each sequence element is updated with a weighted average of all the other elements based on scaled dot-product

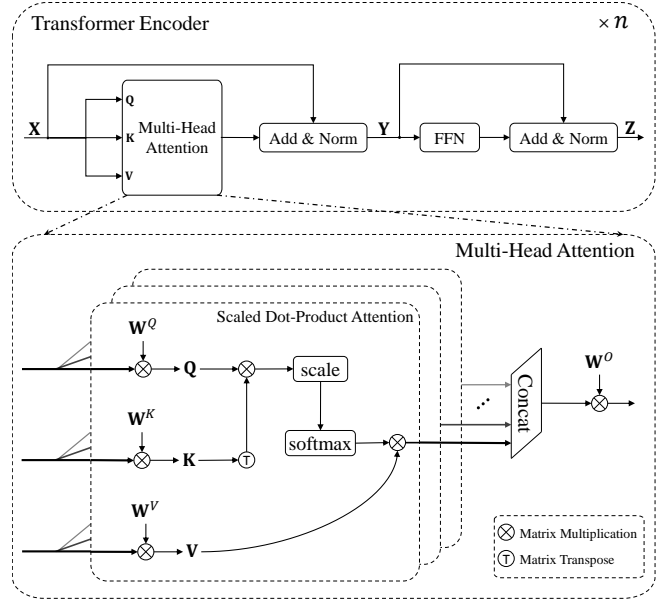


Fig. 4. Architecture of Transformer encoder and Multi-Head Attention. The Transformer encoder layer consists of a Multi-Head Attention layer and a feed-forward network. Stacking multiple encoder layers builds a Transformer encoder. The Multi-Head Attention concatenates and fuses the outputs from multiple scaled dot-product attention sub-modules.

similarity. Let's denote the output sequence  $\{x_i\}_{i=1}^{k_1}$  from the multi-block feature fusion module as  $X \in \mathcal{R}^{k_1 \times d}$ . The scaled dot-product attention first maps embeddings to Queries ( $Q \in \mathcal{R}^{k_1 \times d_s}$ ), Keys ( $K \in \mathcal{R}^{k_1 \times d_s}$ ) and Values ( $V \in \mathcal{R}^{k_1 \times d_s}$ ) with three learnable projection matrices. After that, the similarity between Queries and Keys aggregates Values together,

$$\text{Attention}(Q, K, V) = \text{softmax}\left(\frac{QK^T}{\sqrt{d_s}}\right)V \quad (4)$$

The multi-head structure refers to concatenate the outputs from multiple scaled dot-product attention modules and fuse them with a learnable projection  $W^O$ . It encapsulates complex relationships amongst different elements in the sequence by forcing each head to focus on some specific parts of the input embeddings. The output is added to  $X$  and finally normalized via Layer Normalization (LN),

$$Y = \text{LN}(X + \text{MHA}(Q, K, V)) \quad (5)$$

Besides MHA, the Transformer encoder layer contains a position-wise feed-forward network for non-linearity. It consists of two linear transformations with a ReLU activation,

$$\text{FFN}(Y) = \text{ReLU}(YW_1 + b_1)W_2 + b_2 \quad (6)$$

The final output of one complete Transformer encoder layer is

$$Z = \text{LN}(Y + \text{FFN}(Y)) \quad (7)$$

Following the original structure, we stack  $n$  Transformer encoder layers for the context aggregation purpose. The number of heads in MHA is controlled by a hyper-parameter  $h$ . We name this encoder as BaseEncoder.

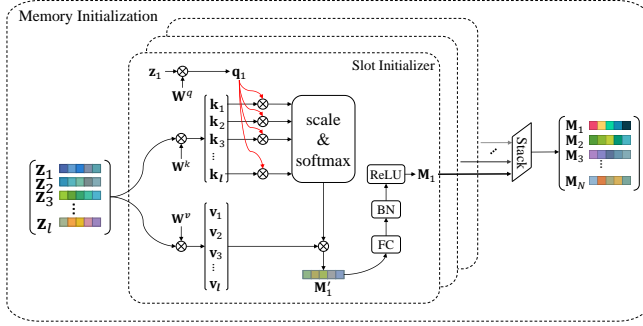


Fig. 5. Memroy initialization.  $\{\mathbf{z}_i\}_{i=1}^{k_1}$  denote the output embeddings from BaseEncoder. Multiple memory slots are stacked to form a complete memory cell.

3) *Memory Initialization*: The Contextual Memory collects different aspects of the probe image, like appearance in different angles, under different illuminations, etc. In other words, the memory cell is an augmented probe embedding with information from multiple images. It mimics the summarization ability of humans for re-ID and re-ranking. To achieve this, we aggregate the probe-related contextual features from local neighbors with attention, which is illustrated in Fig. 5.

The attention first maps  $\mathbf{Z}$  to Queries, Keys, and Values. Instead of producing query vectors for all the elements, we only consider the probe embedding  $\mathbf{z}_1$ . This restriction guides our model to collect the probe-specific features from the local neighbors. Denote three transformation matrices as  $\mathbf{W}^q \in \mathcal{R}^{d \times d_m}$ ,  $\mathbf{W}^k \in \mathcal{R}^{d \times d_m}$  and  $\mathbf{W}^v \in \mathcal{R}^{d \times d_m}$  where  $d_m$  is the sub-feature dimension and  $d_m$  is smaller than  $d$ . The transformation can be formulated as,

$$\begin{aligned} \mathbf{q} &= \mathbf{z}_1 \mathbf{W}^q \\ \mathbf{K} &= \mathbf{Z} \mathbf{W}^k \\ \mathbf{V} &= \mathbf{Z} \mathbf{W}^v \end{aligned} \quad (8)$$

We choose dot-product for similarity calculation and normalize them with softmax,

$$\begin{aligned} \mathbf{M}'_i &= \text{softmax}\left(\frac{\mathbf{q} \mathbf{K}^T}{\mu}\right) \mathbf{V} \\ &= \text{softmax}\left(\frac{\mathbf{z}_1 \mathbf{W}^q (\mathbf{Z} \mathbf{W}^k)^T}{\mu}\right) \mathbf{Z} \mathbf{W}^v \end{aligned} \quad (9)$$

Here,  $\mu$  is a learnable scale parameter which controls the non-linearity of softmax. Finally, we insert a fully connected layer together with batch normalization and ReLU activation after attention. Thus, a memory slot  $\mathbf{M}_i$  is generated by,

$$\mathbf{M}_i = \text{ReLU}(\text{BN}(\mathbf{M}'_i \mathbf{W} + \mathbf{b})) \quad (10)$$

The fully connected layer expands  $\mathbf{M}'_i$  back to the original embedding dimension. As shown in Fig. 5, the memory cell comprises  $N$  independent memory slots.

4) *Memory Refinement*: The memory refinement scheme is proposed to eliminate the feature pollution from noisy false matches. Different from other neural memory networks [38], [39] whose memory writing or updating loops samples in a sequence one by one, we update  $\mathbf{M}$  through the attention between the memory cell and top-ranked highly-confident samples accelerated with parallelization.

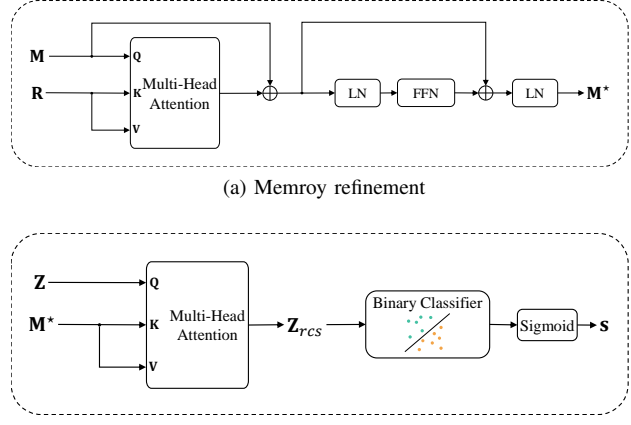


Fig. 6. (a) Memory refinement updates the memory cell by aggregating relevant information from the refinement sequence. (b) Feature reconstruction reversely builds each feature embedding through a combination of multiple memory slots. The binary classifier separates the reconstructed embeddings predicting the correlations.

As mentioned above,  $\mathbf{M}$  aggregates multiple aspects information of a probe from  $\mathbf{Z}$ . The discriminability relies on the dot-product similarity between  $\mathbf{q}$  and  $\mathbf{K}$  in Eq. (9). False matches might be transferred into  $\mathbf{M}$  with low-quality attention weights, which affects the subsequent feature reconstruction and correlation prediction. Hence, we add a memory refinement module after initialization as shown in Fig. 6a. Given the BaseEncoder output sequence  $\mathbf{Z}$ , we chuck it into two parts with the upper part as  $\mathbf{R} = \{\mathbf{z}_i\}_{i=1}^{k_2}$ . The sequence  $\mathbf{R}$  is named as refinement sequence which includes the first  $k_2$  samples of  $\mathbf{Z}$  ( $k_2$  nearest neighbors of the probe). Our memory refinement combines features through attention which converts  $\mathbf{M}$  to Queries, and  $\mathbf{R}$  to Keys and Values. One thing worth mentioning is that the softmax here in MHA is applied on the  $k_2$  dimension of  $\mathbf{R}$ . In other words, each memory slot refines itself by extracting information of interest from the refinement sequence. Memory initialization and refinement cooperate to exclude interfering features of falsely retrieved samples from entering the memory cell. We use this discriminative Contextual Memory  $\mathbf{M}^*$  for feature reconstruct and correlation prediction afterward.

5) *Feature Reconstruction and Correlation Prediction*: The goal of ACP is to accurately predict the correlations between an image and its local neighbors. Since features stored in the memory cell are probe-specific, neighbors reconstructed from the memory will exhibit distinct patterns relevant to their identities. In other words, falsely retrieved samples after reconstruction will be different from those correct matches because they share less common features with the memory. A binary classifier can leverage the feature divergence to distinguish correct matches from strong distractors, predicting the correlations.

The implementation of feature reconstruction is shown in Fig. 6b. The MHA compares the similarity between each neighbor and the Contextual Memory, which can be regarded as the reverse process of the memory initialization (see Fig. 5). Likewise, a learnable projection maps the  $\mathbf{Z}$  to Queries, and the other two projections convert  $\mathbf{M}^*$  to Keys and Values. Each

TABLE I

RE-ID DATASETS STATISTICS. ‘IDS’ DENOTES THE NUMBER OF DIFFERENT IDENTITIES. ‘IMGS’ REPRESENTS THE NUMBER OF CAPTURED IMAGES. ‘CAMS’ REFERS TO THE NUMBER OF UNIQUE CAMERAS. ‘S’, ‘M’ AND ‘L’ INDICATE THREE DIFFERENT TEST SET PARTITIONS NAMELY SMALL, MEDIUM AND LARGE FOR VERI-WILD AND VEHICLEID.

		ReID Datasets												
Splits		VeRi-776			VERI-Wild			VehicleID				Market1501	DukeMTMC	MSMT17
Train	IDs	576	30671		13164		751	702	1041					
	Imgs	37746	277797		113346		12936	16522	30248					
	Cams	20	173		/		6	8	15					
Query	IDs	200	S 3000	M 5000	L 10000	S 800	M 1600	L 2400	750	702	3060			
	Imgs	1678	3000	5000	10000	800	1600	2400	3368	2228	11659			
	Cams	19	105	113	126	/	6	8	15					
Gallery	IDs	200	3000	5000	10000	800	1600	2400	751	1110	3060			
	Imgs	11579	38861	64389	128517	5693	11777	17377	15913	17661	82161			
	Cams	19	146	153	161	/	6	8	15					

feature embedding is reconstructed by finding a combination of multiple memory slots. Let us denote the reconstruction output as  $\mathbf{Z}_{rcs}$ . Unlike Transformer encoder layers where attention outputs are added to the input sequence as residuals, we keep the attention outputs as the final reconstruction results because we reconstruct features for correlation prediction rather than updating the input sequence.

Finally, a binary classifier separates the reconstructed embeddings. Denote the weight matrix of the classifier as  $\mathbf{W}_c \in \mathcal{R}^{d \times 1}$ , and the bias as  $b_c$ . The correlations prediction is,

$$\mathbf{s} = \text{Sigmoid}(\mathbf{Z}_{rcs} \mathbf{W}_c + b_c), \mathcal{R}^{k_1 \times d} \rightarrow \mathcal{R}^{k_1} \quad (11)$$

where  $\text{Sigmoid}(\cdot)$  is the element-wise sigmoid activation. We choose Focal Loss [40] to supervise the network training.

## IV. EXPERIMENTS

### A. Datasets and Evaluation metrics

1) *Datasets*: We evaluate the proposed method on six widely-used re-ID datasets including three person re-ID datasets, i.e., Marker1501 [19], DukeMTMC-ReID [20] and MSMT17 [16] as well as three vehicle re-ID datasets, i.e., VERI-Wild [15], VehicleID [17] and VeRi-776 [18]. An overall statistical comparison on identities, images, and cameras of the datasets is in Table I. Especially, MSMT17 and VERI-Wild are closer to real-world scenarios because of the large number of images, cameras, and unique identities. For example, VERI-Wild is collected from a CCTV surveillance system consisting of 174 cameras over one month under unconstrained conditions. The MSMT17 contains both indoor and outdoor cameras operating at multiple time slots, resulting in severe lighting changes.

2) *Evaluation Metrics*: Following [19], we choose two metrics to evaluate the re-ID performance. Cumulated Matching Characteristics (CMC) measures the probability that the ground-truth appears in the top- $k$  of the ranking list. Here, we report CMC@1 which is generally considered as a reflection of the ability to retrieve the easiest samples. Mean average precision (mAP) calculates the averaged area under the Precision-Recall curve of all the query images. It measures the ability to retrieve all related images.

### B. Implementation Details

1) *Re-ID Baseline*: The baseline network is proposed by [5] which adopts a single-branch ResNet-50 as the backbone

TABLE II

HYPER-PARAMETERS FOR MODEL ARCHITECTURES, TRAINING AND TESTING. THE  $\gamma$  BELONGS TO FOCAL LOSS.

	Model Architeture						Training			Testing	
	$d$	$h$	$d_m$	$p_d$	$n$	$N$	$l_1$	$l_2$	$\gamma$	$k_1$	$k_2$
Market1501	256	8	64	0.5	3	8	80	32	2	20	6
DukeMTMC	256	8	64	0.5	3	8	80	32	2	20	6
MSMT17	256	8	64	0.3	3	8	80	32	1	25	6
VeRi-776	256	8	64	0.5	3	8	160	64	2	55	10
VehicleID	256	8	64	0	3	8	24	8	1	25	4
VERI-Wild	1024	16	128	0	3	8	32	8	1	25	6

feature extractor. In general, the strong baseline uses several following techniques to stabilize training and improve performance. For example, Learning Rate Warm-Up increases the learning rate linearly in the initial training stage to slow down over-fitting and maintain the stability of deeper layers. Batch Normalization (BN) Neck relieves the inconsistency between cross-entropy identity loss and triplet loss. Random Erasing Augmentation (REA) and Label Smoothing both aim at reducing over-fitting and encouraging robust features. The implementation comes from FastReID <sup>1</sup> [14] which is a powerful open-source toolbox designed for general instance re-ID.

2) *Attention-based Correlation Predictor*: The model architecture and the training process are controlled by several hyper-parameters as shown in Table II. To construct a training sequence, we find the  $K = 1000$  nearest neighbors for each image. Suppose there are  $m$  correct matches and  $K - m$  false matches. We randomly select  $l_1$  samples from the union set of the correct matches and the first several false matches. The refinement sequence length is set to  $l_2$ . The model training adopts Adam optimizer with weight decay as  $5 \times 10^{-4}$ . The initial learning rate is set to  $2 \times 10^{-4}$ . Similar to [5], we linearly warm up the learning process for the first 10 epochs with warm-up factor equals 0.1. The parameter  $\gamma$  in Focal loss balances easy and hard samples. For MSMT17, VehicleID, and VERI-Wild, we choose  $\gamma = 1$ , making the Focal loss degrade to cross-entropy loss. We find this setting slightly improves the performance on three larger datasets. The testing parameters  $k_1$  and  $k_2$  are determined based on the test set size, empirically. All the experiments are conducted on a platform with 256GB RAM and  $2 \times$  Intel Xeon Silver 4214R CPU @ 2.40GHz. The GPU we use is a single GeForce RTX 2080Ti with 11GB VRAM.

### C. Performance Comparison

In this subsection, we compare the performance of our re-ranking approach with several widely-used re-ranking methods on the datasets mentioned above. Results are reported and analyzed in Section IV-C1. We choose parameters based on the recommendations tested in their original papers. Because re-ranking methods are generally sensitive to parameter selection, we also studied the influence of hyper-parameters in Section IV-C2.

<sup>1</sup><https://github.com/JDAI-CV/fast-reid>

TABLE III  
PERFORMANCE (%) COMPARISON. THE BEST AND SECOND-BEST RESULTS ARE MARKED IN RED AND BLUE, RESPECTIVELY.

Method	MSMT17		VeRi-776		VERI-Wild						VehicleID						Market1501		DukeMTMC					
	CMC@1 mAP		CMC@1 mAP		Small			Medium			Large			Small			Medium			Large			CMC@1 mAP	CMC@1 mAP
	CMC@1	mAP	CMC@1	mAP	CMC@1	mAP	CMC@1	CMC@1	mAP	CMC@1	CMC@1	CMC@1	mAP	CMC@1	CMC@1	CMC@1	CMC@1	CMC@1	CMC@1	CMC@1	CMC@1	CMC@1	CMC@1	
Baseline	73.75	50.31	96.07	78.56	93.27	76.74	90.04	70.61	86.52	62.56	82.82	95.50	77.51	91.23	75.57	88.97	93.85	86.31	86.36	76.98				
AQE	76.82	64.26	96.01	84.54	85.41	71.64	81.04	65.51	76.20	56.64	71.83	89.69	65.83	85.12	65.80	85.05	94.24	91.85	89.95	86.56				
$\alpha$ QE	79.04	65.42	97.44	85.95	92.67	79.37	89.50	72.75	85.59	63.92	84.72	96.54	77.47	91.65	76.64	90.47	95.37	93.08	90.22	86.92				
$k$ -reciprocal	78.92	67.12	96.54	85.61	93.84	80.32	90.66	73.94	87.09	65.65	84.00	95.43	77.34	90.47	75.68	88.31	95.34	93.98	90.53	88.93				
$\alpha$ QE + $k$ -reciprocal	78.83	69.94	96.90	87.58	91.83	78.94	88.01	72.18	82.80	63.15	83.23	95.63	76.48	91.09	75.35	89.50	95.37	93.97	90.26	89.15				
SCA	79.10	69.08	96.60	84.52	92.77	79.65	89.52	73.30	-	-	82.54	93.98	76.12	87.81	74.85	86.91	95.19	94.14	90.04	89.34				
GNN	-	-	96.84	86.10	-	-	-	-	-	-	82.79	94.20	76.79	88.66	75.40	88.02	95.34	94.55	90.71	90.03				
ECN	-	-	97.14	85.52	90.63	79.68	-	-	-	-	77.25	92.66	72.85	87.55	71.48	86.45	95.61	94.47	91.11	89.71				
Ours	82.00	72.11	97.02	87.50	95.18	88.16	92.45	83.60	89.64	75.80	88.13	97.10	82.12	93.74	81.66	91.73	95.49	93.95	90.98	89.08				

1) *Comparisons with State-of-the-art Methods*: The experimental results for each method are listed in Table III. We tested AQE [8],  $\alpha$ QE [9],  $k$ -reciprocal [12], SCA [27], GNN [30] and ECN [23]. The row named ‘ $\alpha$ QE +  $k$ -reciprocal’ refers to perform  $k$ -reciprocal re-ranking after  $\alpha$ QE. For GNN, ECN and SCA re-ranking, some results are not available because of insufficient memory. Note that the implementation of AQE and  $\alpha$ QE here expand all the feature embeddings by considering the query and gallery sets as a whole.

**MSMT17** is the largest person re-ID dataset in our experiments, especially for the test set which adds up to almost 100k images in total. As shown in Table III, we ranked first for both CMC@1 and mAP. The baseline CMC@1 improved from 73.75% to 82.00%, and baseline mAP increased to 72.11% from 50.31% with 21.80% improvement. The improvement proves that our method is better at handling complex relationships between the  $k$ -nearest neighbors. Besides, we only require the access of first-order nearest neighbors for each probe embedding.

**VeRi-776** has relative more images per identity on average. Therefore, we increase the neighborhood size  $k_1$  accordingly. Results show that we produce the second-best mAP, which equals 87.50%. Although our method does not rank first for CMC@1, there is only 0.42% difference compared to the best result obtained by  $\alpha$ QE. Our method achieved the balance between CMC@1 and mAP.

**VERI-Wild**. We can significantly boost the baseline performance on the small, medium, and large subsets of VERI-Wild. By comparing the results across different subsets, we can observe that the  $k$ -reciprocal rule begins to fails as the testing set becomes larger. The mAP improvements for  $k$ -reciprocal re-ranking are 3.58%, 3.33%, 3.09% for small, medium, and large, respectively. However, our method is robust to the test set size achieving 11.42%, 12.99%, and 13.24%. Some methods run out of memory halfway.

**VehicleID**. The metric mAP is not provided because there is only one correct match in the gallery set for each query image. Instead, we report CMC@5 which measures the probability of having the correct match in top-5 candidates. As shown in the table, our method outperforms other re-ranking approaches for all three subsets by a large margin. The improvement of  $k$ -reciprocal re-ranking is limited, which might be caused by the insufficient contextual information in the gallery set (one image per identity). The  $\alpha$ QE gains a slight improvement over the baseline by taking the query-to-query similarities into account. The comparison between  $\alpha$ QE and our approach demonstrates

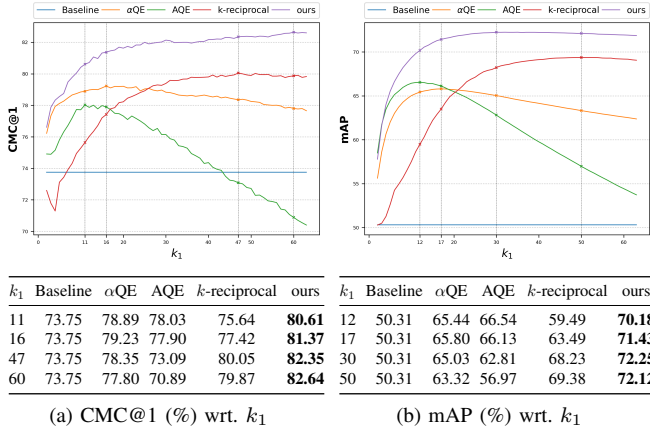
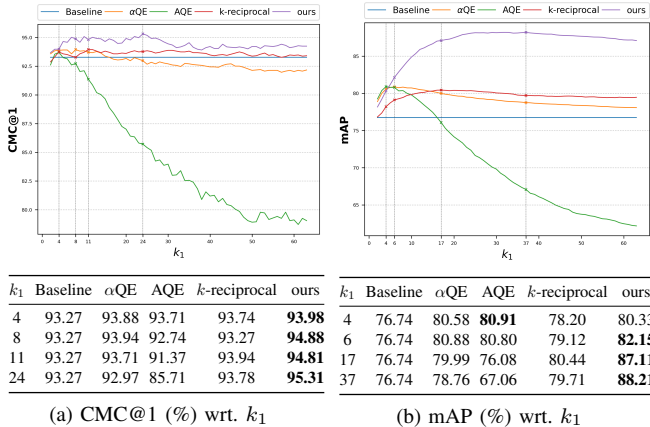
the superiority of discriminative correlation prediction.

**Market1501**. Our method achieves the second-best CMC@1, which equals 95.49% with only 0.12% difference compared to the best obtained by ECN re-ranking. For mAP, the best result 94.55% is produced by GNN re-ranking, which is 0.6% higher than ours. We ascribe this unsatisfying result to the lack of training data. As shown in Table I, Market1501 is the smallest amongst all six datasets with only 13k images for training. The backbone itself has already been facing over-fitting problems, not even for building a re-ranking network without extra training data.

**DukeMTMC**. Similar to Market1501, our approach ranked second for CMC@1. We obtain 90.98% which is 0.13% lower than the best 91.11%. We consider the inferior results are mainly caused by three facts. First of all, DukeMTMC has less than 17k images for training with only 3586 additional images compared to the Market1501. Second, the test sets for both benchmarks are relatively simpler than others. Images are taken under 6 and 8 cameras for the Market1501 and DukeMTMC, respectively. The limited cameras indicate the limited appearance variation within an identity. Last, unique identities are less than 800, which reduces the probability of having strong similar persons. Therefore, the neighborhood relationships of Market1501 and DukeMTMC are less complex than MSMT17 and VERI-Wild. This kind of simplicity can be well modeled by hand-designed algorithms but imposes over-fitting risks on our deep learning-based approach. For mAP, all the methods bring considerable improvements, and our approach is 12.10% higher than the baseline. The highest mAP is produced by ECN re-ranking.

2) *Parameter Sensitivity*: Here, we study the influence of the testing parameters  $k_1$  and  $k_2$ .

**Neighborhood size  $k_1$** . We use  $k_1$  to control the number of nearest neighbors. Generally, larger  $k_1$  means richer contextual information but also involves more false matches. The previous section tests the performance with empirically decided parameters, which may not fully reveal the maximum capacity for each method. For example,  $\alpha$ QE can leverage contextual cues in broader neighborhoods than AQE because of the power-normalized combination weight. To better study the influence of neighborhood size, we evaluate re-ranking methods via gradually increasing  $k_1$ . The performance variation is compared amongst AQE,  $\alpha$ QE,  $k$ -reciprocal re-ranking, and our method. We fix the  $\alpha$  in  $\alpha$ QE as 3 and  $\lambda$  in  $k$ -reciprocal re-ranking as 0.3. Because of the space limitation, we only show the figures for MSMT17 in Fig. 7 and the small subset of

Fig. 7. Performance versus  $k_1$  on MSMT17.Fig. 8. Performance versus  $k_1$  on the small subset of VERI-Wild.

VERI-Wild in Fig. 8. The  $k_2$  is fixed as 6 for both datasets. We list the peak performance below in a table with the best result in each row marked with bold type. From the curve plots, we have the following observations. First, the performance of AQE drops quickly as  $k_1$  becomes larger because AQE assigns uniform weight to each neighbor. The aggregated feature embedding will be pulled towards the wrong directions if false matches dominate the neighborhood. The  $\alpha$ QE uses power-normalized combination weights, which significantly relieves the false-match pollution issue. However, it is still not enough to entirely reject falsely retrieved samples resulting in the gradual performance degeneration. Second, our approach consistently outperforms  $\alpha$ QE for CMC@1 and mAP with a large margin. Given a specific  $k_1$ , the performance gap proves that the correlation prediction provides a more accurate direction to shrink embeddings toward their identity centers. Third, compared to  $\alpha$ QE, the  $k$ -reciprocal rule with backward verification is more robust to false matches. The turning point of  $k$ -reciprocal re-ranking where the performance begins to drop comes later than  $\alpha$ QE.

**Refinement sequence  $k_2$ .** As mentioned above, memory refinement reduces feature pollution from falsely aggregated neighbors using a small group of high-confident samples. To measure the sensitivity, we test the performance of our method

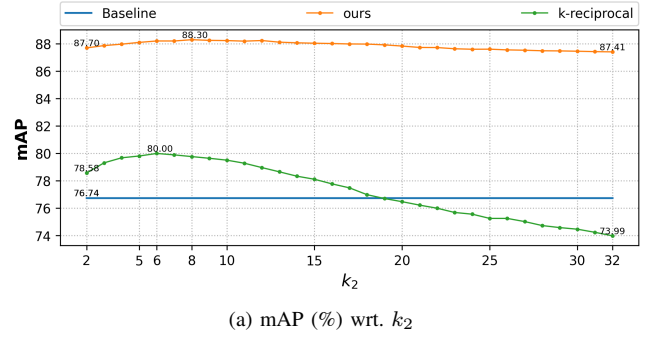
(a) mAP (%) wrt.  $k_2$ Fig. 9. Performance variation versus  $k_2$  for  $k$ -reciprocal re-ranking and our method.

TABLE IV

ABLATION STUDY. IN THE FIRST ROW, EXPERIMENTS ARE TAGGED WITH EXP- $X$  WHERE  $X$  IS A CAPITAL LETTER. THE BEST AND SECOND BEST RESULTS ARE MARKED IN RED AND BLUE RESPECTIVELY.

Modules	Baseline	Exp-A	Exp-B	Exp-C	Exp-D	Exp-E	Exp-F	Exp-G
Multi-Block Feature Fusion			✓	✓			✓	✓
BaseEncoder			✓	✓	✓			✓
Memory cell				✓	✓	✓	✓	✓
Memory refinement					✓	✓	✓	✓
CMC@1	93.27%	86.18%	86.98%	92.87%	92.07%	<b>94.38%</b>	93.37%	<b>95.18%</b>
mAP	76.74%	77.93%	77.90%	86.31%	84.20%	<b>87.09%</b>	86.56%	<b>88.16%</b>

on the small subset of VERI-Wild with different  $k_2$ . Fig. 9 shows the variation with  $k_1$  fixed as 32.

The result shows that mAP increases as the refinement sequence becomes longer, starting from a small value. We reach the best mAP when refining on the 8-nearest neighbors. After that, mAP gradually drops if we continue to include more samples. Compared to the best result 88.30%, mAP drops to 87.41% when  $k_2 = 32$ , which is even worse than  $k_2 = 2$  whose mAP reaches 87.70%. This indicates that a small group of highly-confident neighboring embeddings are helpful in improving the discriminability of memory. We also plot the performance of  $k$ -reciprocal re-ranking versus  $k_2$  in Fig. 9 which controls the local query expansion. The decrease of mAP shows that it is more sensitive to  $k_2$  because of its indiscriminate combination.

#### D. Model Studies

In this section, we study the influence of model architectures. Specifically, we verify the effectiveness of the proposed modules in Section IV-D1 by conducting ablation experiments. Besides, we test how the model architecture parameters, such as the number of heads in MHA, affect the final result in Section IV-D2.

1) **Ablation:** The proposed model comprises multiple modules, i.e., multi-block feature fusion, BaseEncoder, Contextual Memory, and memory refinement. We train the model until convergence with one or multiple modules removed. The re-ranking performance is tested on the small subset of VERI-Wild with  $k_1 = 25, k_2 = 6$ . Results are shown in Table IV. Note that the output from BaseEncoder will be fed into the final binary classifier if the memory cell is disabled.

**Multi-Block Feature Fusion.** We conducted two experiments (Exp-E and Exp-G) to study whether features from

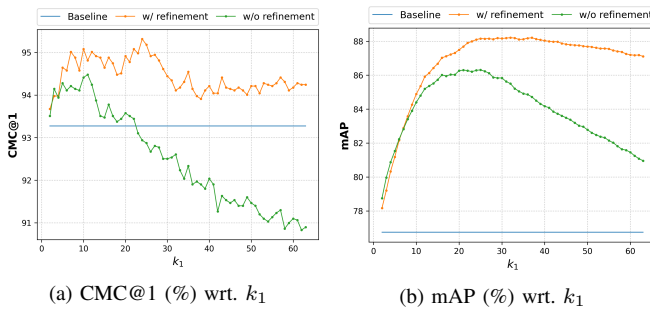


Fig. 10. Ablation study with memory refinement module removed.

shallower layers contain discriminative information. Results show the CMC@1 and mAP improve from 94.38% to 95.18% and 87.09% to 88.16%, respectively. The improvement verifies our assumption that different blocks provide information in various granularities. Our re-ranking approach can make use of this information that is discarded in the baseline model.

**BaseEncoder.** Before memory initialization, multi-block features are preprocessed by the BaseEncoder which aggregates the contextual information for each embedding. Comparing Exp-F and Exp-G, we can observe that CMC@1 and mAP drop 1.81% and 1.60% respectively with BaseEncoder disabled. However, the decline is more severe if multi-block feature fusion is removed at the same time. From Exp-E to Exp-D, the CMC@1 and mAP decrease 2.31% and 2.89%, respectively. A possible explanation is that the multi-block feature vector provides richer information than the baseline. Once discriminative features from shallower blocks are cut off, the ability of BaseEncoder to aggregate homogeneous sub-features plays an important role.

**Contextual Memroy** is the most critical module in our architecture. As shown in Exp-B and Exp-C, directly predicting correlations for embeddings generated by BaseEncoder significantly harms the performance. The CMC@1 decreases from 92.87% to 86.98% with 5.89% decline. Similarly, mAP also drops 8.41%, reaching 77.90%. The performance drop suggests that a fixed hyperplane is not enough to separate embeddings from Transformer encoder. Instead, the similarity between each embedding counts.

**Memory refinement** is a sub-module of the Contextual Memory which aims at preventing feature pollutions. We conduct Exp-C and Exp-G to study the refinement process with  $k_1$  fixed as 25. The CMC@1 increases from 92.87% to 95.18% with 2.31% improvement and mAP also improved 1.85%. To better reveal the power of memory refinement, we evaluate the re-ranking performance under different  $k_1$  for the consideration that refinement is more crucial if more false matches are included in the neighborhood. The metric curve versus  $k_1$  is shown in Fig. 10. Comparing the results, we can observe that the model without refinement deteriorates rapidly when  $k_1$  becomes larger. Memory refinement enables our model to leverage contextual information in larger neighborhoods without affected by false matches.

2) *Model Architecture Parameters:* The ablation studies verify the effectiveness of each proposed module. Here, we

TABLE V  
PERFORMANCE VARIATION WRT. NUMBER OF ENCODER LAYERS IN THE BASEENCODER.

Layers	1	2	3	4	5	6
CMC@1(%)	94.14	95.18	95.18	94.78	94.65	94.31
mAP(%)	87.22	88.21	88.16	88.14	88.10	87.75

TABLE VI  
PERFORMANCE VARIATION WRT. NUMBER OF HEADS IN MHA.

Heads	1	2	4	8	16	32	64	128
CMC@1(%)	92.03	92.00	93.47	94.24	95.18	94.61	94.61	94.54
mAP(%)	84.28	83.77	85.98	87.01	88.16	87.97	88.02	87.94

perform experiments to study the relationships between architecture parameters and the re-ranking performance. The basic model follows Exp-G in Table IV with all the modules enabled. Each time, we set different values for an architecture parameter with others fixed. After the model converges, CMC@1 and mAP are tested on the small subset of VERI-Wild with  $k_1 = 25, k_2 = 6$ .

**BaseEncoder Layers.** We control the model capacity by adjusting the number of layers in the BaseEncoder. Results are shown in Table V. We can observe that the two-layer BaseEncoder obtains the best results. If we stack more layers, the performance gradually decreases but is relatively stable. At the same time, we noticed that the model becomes harder to converge. The warm-up period is doubled to 20 epochs to stabilize the model at initial training stages for 4-layer, 5-layer, and 6-layer BaseEncoder. The model degeneration is likely to be caused by that deeper BaseEncoder affects the backflow of gradient.

**Heads in Multi-Head Attention.** MHA is one of the important building blocks in our model. The head refers to split original feature embeddings into multiple smaller ones for attention calculation independently. As shown in Table VI, results are unsatisfying for models with limited number of heads. For example, the CMC@1 drops from 95.18% to 92.03% when heads reduce from 16 to 1. The mAP also drops 3.88%. Intuitively, the multi-head structure captures the similarity between different sub-features. It can be considered an improved version of [28] where sub-features are selected either manually or randomly. The projection matrices in Multi-Head Attention are learned from data, which enable the transformed sub-features to focus on the most discriminative regions.

**Memory Size** refers to the number of slots in the Contextual Memory. Similar to the Multi-Head Attention, each memory slot focuses on some specific aspects. Therefore, the memory size relates to the distinctive aspects of a person or vehicle. We study the memory size in Table VII. From the table, the eight-slot memory outperforms others. An interesting finding is that the number 8 happens to be the same as the views in multi-view feature inference [7], which suggests the memory cell stores view-related information inside. Further increasing the memory size slightly harms the performance. However, the effect is more significant if we adopt a smaller memory. The

TABLE VII  
PERFORMANCE VARIATION WRT. THE MEMORY SIZE.

Memory Size	2	4	8	12	16	20	24	28	32
CMC@1(%)	93.71	94.51	95.18	94.98	94.95	94.88	94.48	94.28	94.68
mAP(%)	86.43	87.51	88.16	87.98	87.87	87.88	87.69	87.49	87.52

CMC@1 decreases 1.47% and mAP drops 1.73% from eight-slot memory to tow-slot memory because small Contextual Memory can not provide enough discriminative features for neighborhood reconstruction.

## V. CONCLUSION

In this paper, we have proposed a novel Contextual Memory cell to mimic the remembering process that humans adopt for re-ID and re-ranking. By comparing neighbors' features with the multi-view appearance information in the memory, we predict the correlations between each image and its  $k$ -nearest neighbors. The re-ranking is achieved by shrinking each embedding towards the identity centers with correlation prediction as discriminative combination weights. Experiments on six widely-used re-ID datasets validate the effectiveness of the proposed method. Especially, the performance boost on large-scale datasets VERI-Wild, MSMT17, and VehicleID exhibits the ability of ACP in handling complex neighborhood relationships.

## REFERENCES

- [1] M. Ye, C. Liang, Y. Yu, Z. Wang, Q. Leng, C. Xiao, J. Chen, and R. Hu, "Person reidentification via ranking aggregation of similarity pulling and dissimilarity pushing," *IEEE Transactions on Multimedia*, vol. 18, no. 12, pp. 2553–2566, 2016. [1](#), [3](#)
- [2] Z. Zheng, T. Ruan, Y. Wei, Y. Yang, and T. Mei, "Vehiclenet: learning robust visual representation for vehicle re-identification," *IEEE Transactions on Multimedia*, 2020. [1](#)
- [3] F. Xiong, M. Gou, O. Camps, and M. Sznaier, "Person re-identification using kernel-based metric learning methods," in *European conference on computer vision*. Springer, 2014, pp. 1–16. [1](#)
- [4] T. Matsukawa, T. Okabe, E. Suzuki, and Y. Sato, "Hierarchical gaussian descriptor for person re-identification," in *Proceedings of the IEEE conference on computer vision and pattern recognition*, 2016, pp. 1363–1372. [1](#)
- [5] H. Luo, W. Jiang, Y. Gu, F. Liu, X. Liao, S. Lai, and J. Gu, "A strong baseline and batch normalization neck for deep person re-identification," *IEEE Transactions on Multimedia*, vol. 22, no. 10, pp. 2597–2609, 2019. [1](#), [2](#), [6](#)
- [6] P. Khorramshahi, N. Peri, J.-c. Chen, and R. Chellappa, "The devil is in the details: Self-supervised attention for vehicle re-identification," in *European Conference on Computer Vision*. Springer, 2020, pp. 369–386. [1](#), [2](#)
- [7] Y. Zhou, L. Liu, and L. Shao, "Vehicle re-identification by deep hidden multi-view inference," *IEEE Transactions on Image Processing*, vol. 27, no. 7, pp. 3275–3287, 2018. [1](#), [2](#), [9](#)
- [8] O. Chum, J. Philbin, J. Sivic, M. Isard, and A. Zisserman, "Total recall: Automatic query expansion with a generative feature model for object retrieval," in *2007 IEEE 11th International Conference on Computer Vision*. IEEE, 2007, pp. 1–8. [1](#), [2](#), [7](#)
- [9] F. Radenović, G. Tolias, and O. Chum, "Fine-tuning cnn image retrieval with no human annotation," *IEEE transactions on pattern analysis and machine intelligence*, vol. 41, no. 7, pp. 1655–1668, 2018. [1](#), [2](#), [7](#)
- [10] R. Arandjelović and A. Zisserman, "Three things everyone should know to improve object retrieval," in *2012 IEEE Conference on Computer Vision and Pattern Recognition*. IEEE, 2012, pp. 2911–2918. [1](#), [2](#)
- [11] M. Ye, J. Chen, Q. Leng, C. Liang, Z. Wang, and K. Sun, "Coupled-view based ranking optimization for person re-identification," in *International Conference on Multimedia Modeling*. Springer, 2015, pp. 105–117. [1](#)
- [12] Z. Zhong, L. Zheng, D. Cao, and S. Li, "Re-ranking person re-identification with k-reciprocal encoding," in *Proceedings of the IEEE Conference on Computer Vision and Pattern Recognition*, 2017, pp. 1318–1327. [1](#), [3](#), [7](#)
- [13] Y. Sun, L. Zheng, Y. Yang, Q. Tian, and S. Wang, "Beyond part models: Person retrieval with refined part pooling (and a strong convolutional baseline)," in *Proceedings of the European conference on computer vision (ECCV)*, 2018, pp. 480–496. [1](#), [2](#)
- [14] L. He, X. Liao, W. Liu, X. Liu, P. Cheng, and T. Mei, "Fastreid: a pytorch toolbox for real-world person re-identification," *arXiv preprint arXiv:2006.02631*, 2020. [1](#), [6](#)
- [15] Y. Lou, Y. Bai, J. Liu, S. Wang, and L.-Y. Duan, "Veri-wild: A large dataset and a new method for vehicle re-identification in the wild," in *Proceedings of the IEEE Conference on Computer Vision and Pattern Recognition*, 2019, pp. 3235–3243. [2](#), [6](#)
- [16] L. Wei, S. Zhang, W. Gao, and Q. Tian, "Person transfer gan to bridge domain gap for person re-identification," in *2018 IEEE/CVF Conference on Computer Vision and Pattern Recognition*, 2018, pp. 79–88. [2](#), [6](#)
- [17] H. Liu, Y. Tian, Y. Wang, L. Pang, and T. Huang, "Deep relative distance learning: Tell the difference between similar vehicles," in *2016 IEEE Conference on Computer Vision and Pattern Recognition (CVPR)*, 2016, pp. 2167–2175. [2](#), [6](#)
- [18] X. Liu, W. Liu, T. Mei, and H. Ma, "Provid: Progressive and multi-modal vehicle reidentification for large-scale urban surveillance," *IEEE Transactions on Multimedia*, vol. 20, no. 3, pp. 645–658, 2017. [2](#), [6](#)
- [19] L. Zheng, L. Shen, L. Tian, S. Wang, J. Wang, and Q. Tian, "Scalable person re-identification: A benchmark," in *Proceedings of the IEEE international conference on computer vision*, 2015, pp. 1116–1124. [2](#), [6](#)
- [20] E. Ristani, F. Solera, R. Zou, R. Cucchiara, and C. Tomasi, "Performance measures and a data set for multi-target, multi-camera tracking," in *European conference on computer vision*. Springer, 2016, pp. 17–35. [2](#), [6](#)
- [21] L. Zheng, H. Zhang, S. Sun, M. Chandraker, Y. Yang, and Q. Tian, "Person re-identification in the wild," in *Proceedings of the IEEE Conference on Computer Vision and Pattern Recognition*, 2017, pp. 1367–1376. [2](#)
- [22] X. Qian, Y. Fu, Y.-G. Jiang, T. Xiang, and X. Xue, "Multi-scale deep learning architectures for person re-identification," in *Proceedings of the IEEE International Conference on Computer Vision*, 2017, pp. 5399–5408. [2](#)
- [23] M. S. Sarfraz, A. Schumann, A. Eberle, and R. Stiefelhagen, "A pose-sensitive embedding for person re-identification with expanded cross neighborhood re-ranking," in *Proceedings of the IEEE Conference on Computer Vision and Pattern Recognition*, 2018, pp. 420–429. [2](#), [3](#), [7](#)
- [24] H. Wang, J. Peng, D. Chen, G. Jiang, T. Zhao, and X. Fu, "Attribute-guided feature learning network for vehicle reidentification," *IEEE MultiMedia*, vol. 27, no. 4, pp. 112–121, 2020. [2](#)
- [25] A. Hermans, L. Beyer, and B. Leibe, "In defense of the triplet loss for person re-identification," *arXiv preprint arXiv:1703.07737*, 2017. [2](#)
- [26] D. Qin, S. Gammeter, L. Bossard, T. Quack, and L. Van Gool, "Hello neighbor: Accurate object retrieval with k-reciprocal nearest neighbors," in *CVPR 2011*. IEEE, 2011, pp. 777–784. [2](#)
- [27] S. Bai and X. Bai, "Sparse contextual activation for efficient visual re-ranking," *IEEE Transactions on Image Processing*, vol. 25, no. 3, pp. 1056–1069, 2016. [3](#), [7](#)
- [28] R. Yu, Z. Zhou, S. Bai, and X. Bai, "Divide and fuse: A re-ranking approach for person re-identification," *arXiv preprint arXiv:1708.04169*, 2017. [3](#), [9](#)
- [29] Z. Wang, J. Jiang, Y. Yu, and S. Satoh, "Incremental re-identification by cross-direction and cross-ranking adaption," *IEEE Transactions on Multimedia*, vol. 21, no. 9, pp. 2376–2386, 2019. [3](#)
- [30] X. Zhang, M. Jiang, Z. Zheng, X. Tan, E. Ding, and Y. Yang, "Understanding image retrieval re-ranking: A graph neural network perspective," *arXiv preprint arXiv:2012.07620*, 2020. [3](#), [7](#)
- [31] A. Vaswani, N. Shazeer, N. Parmar, J. Uszkoreit, L. Jones, A. N. Gomez, L. Kaiser, and I. Polosukhin, "Attention is all you need," *arXiv preprint arXiv:1706.03762*, 2017. [3](#)
- [32] X. Wang, R. Girshick, A. Gupta, and K. He, "Non-local neural networks," in *Proceedings of the IEEE conference on computer vision and pattern recognition*, 2018, pp. 7794–7803. [3](#)
- [33] N. Parmar, A. Vaswani, J. Uszkoreit, L. Kaiser, N. Shazeer, A. Ku, and D. Tran, "Image transformer," in *International Conference on Machine Learning*. PMLR, 2018, pp. 4055–4064. [3](#)
- [34] N. Carion, F. Massa, G. Synnaeve, N. Usunier, A. Kirillov, and S. Zagoruyko, "End-to-end object detection with transformers," in

*European Conference on Computer Vision.* Springer, 2020, pp. 213–229. <sup>3</sup>

- [35] A. Dosovitskiy, L. Beyer, A. Kolesnikov, D. Weissenborn, X. Zhai, T. Unterthiner, M. Dehghani, M. Minderer, G. Heigold, S. Gelly *et al.*, “An image is worth 16x16 words: Transformers for image recognition at scale,” *arXiv preprint arXiv:2010.11929*, 2020. <sup>3</sup>
- [36] S. He, H. Luo, P. Wang, F. Wang, H. Li, and W. Jiang, “Transreid: Transformer-based object re-identification,” *arXiv preprint arXiv:2102.04378*, 2021. <sup>3</sup>
- [37] K. He, X. Zhang, S. Ren, and J. Sun, “Deep residual learning for image recognition,” in *Proceedings of the IEEE conference on computer vision and pattern recognition*, 2016, pp. 770–778. <sup>4</sup>
- [38] Y. Yuan, D. Wang, and Q. Wang, “Memory-augmented temporal dynamic learning for action recognition,” in *Proceedings of the AAAI Conference on Artificial Intelligence*, vol. 33, no. 01, 2019, pp. 9167–9175. <sup>5</sup>
- [39] T. Yang and A. B. Chan, “Visual tracking via dynamic memory networks,” *IEEE transactions on pattern analysis and machine intelligence*, vol. 43, no. 1, pp. 360–374, 2019. <sup>5</sup>
- [40] T.-Y. Lin, P. Goyal, R. Girshick, K. He, and P. Dollár, “Focal loss for dense object detection,” in *Proceedings of the IEEE international conference on computer vision*, 2017, pp. 2980–2988. <sup>6</sup>